Fraunhofer diffraction in the crystalline phases of a monolayer

2002 J. Phys.: Condens. Matter 14 4767

(http://iopscience.iop.org/0953-8984/14/19/303)

INSTITUTE OF PHYSICS PUBLISHING JOURNAL OF PHYSICS: CONDENSED MATTER

J. Phys.: Condens. Matter **14** (2002) 4767–4775 PII: S0953-8984(02)30220-0

Fraunhofer diffraction in the crystalline phases of a monolayer

Julián Galván-Miyoshi and Rolando Castillo[1]

Instituto de Física, UNAM, PO Box 20-364, DF 01000, México

E-mail: rolandoc@fisica.unam.mx

Received 31 October 2001, in final form 21 January 2002
Published 2 May 2002
Online at stacks.iop.org/JPhysCM/14/4767

Abstract

Localized oscillations recently found in crystalline phases of the heneicosanoic acid Langmuir monolayer were studied. They appear like blinking interference rings, when observed with Brewster angle microscopy. The optical analysis of the interference rings is consistent with Fraunhofer diffraction caused by light reflected from multilayer granules formed by material expulsion from the monolayer.

1. Introduction

Amphiphilic molecules of nearly water insoluble molecules form Langmuir monolayers (LMs) at the air–water interface. The most common way of studying these monolayers is through the measurement of surface pressure isotherms $\pi(A, T) = \gamma_0(T) - \gamma(A, T)$, where T is the temperature, A is the area/molecule and γ and γ_0 are the surface tensions of the LM and of pure water, respectively. However, the use of new techniques, such as x-ray diffraction, polarized fluorescence microscopy (PFM) and Brewster angle microscopy (BAM), have contributed to obtain a general picture of the fatty acid LMs, as well as the structure of their phases [1]. This picture can be reviewed as follows: at very low surface densities, when the average area per molecule, a, is much larger than the cross section area of an isolated molecule, an amphiphilic monolayer behaves as a two-dimensional gas. A first-order phase transition from the gas phase to a liquid-expanded phase is observed upon compression of the monolayer. This phase is isotropic and molecules are tilted, although this tilting is not correlated [2]. A second phase transition to a liquid condensed state is observed upon further compression of the monolayer. Here, A is just barely larger than the cross sectional area of a fully stretched (all-*trans*) chain. Actually, the liquid condensed phase is made up of a variety of mesophases, i.e. phases where the translational order of the molecules is short ranged and the orientational order of the bonds between the molecules is of quasi-long range. At low surface pressures, there are several mesophases showing molecular tilt with distinct symmetry. The L_2 phase

[1] Author to whom any correspondence should be addressed.

has a collective tilt towards a nearest neighbour (NN) [3–9]. The phases L_2' and Ov tilt to a next-nearest-neighbour (NNN) molecule [3–5, 7–9]. At high pressure, there are two untilted mesophases, the super liquid phase, LS, [5, 6, 10, 11], and the solid phase, S [3, 5, 10, 12]. The structure of these mesophases can be locally hexagonal (LS) or distorted hexagonal, i.e. centred rectangular (L_2, L_2', Ov, S). In addition to mesophases, crystalline phases have been found with a positional quasi-long-range order. They are CS and L_2'' phases, which are centred rectangular with herringbone order. L_2'' is a two-dimensional crystal with an NN tilt [3] and CS is untilted [3, 7, 8, 11, 12]. Textures of condensed phases and the precise coexistence lines between phases have been obtained mainly using PFM and BAM [13–16]. At very high pressures, i.e. when A or π reach a limiting value beyond which the monolayer cannot be further compressed, all phases collapse in multilayers. LMs can fracture and break as usually seen with BAM in S and CS phases; buckle at constant area [17]; form folds or ridges [18], packing defects [19] etc. The different ways of collapse, as well as the details of the multilayering process, are quite unknown. Some mechanisms for the collapse have been proposed [18, 21] and similarities have been suggested [20].

A different multilayering process, where material is abruptly ejected from the monolayer, below the collapse pressure, has been reported by some of us using BAM [16]. In crystalline phases L_2'' and CS of the heneicosanoic acid (C_{21}) LM, it has been possible to observe with BAM something that reminds us of interference rings, which are blinking. They suddenly appear and completely disappear in the same place on the monolayer; they have been called *localized oscillations* (LOs) [16]. When they are not blinking, they have been colloquially named Newton rings by the LM community. Here, we shall present a series of experiments to show the behaviour of these LOs in monolayers which were prepared in different conditions. In addition, we present a model that explains the origin of the interference patterns, as well as a series of experiments to support this model. However, although many of the features of these LOs could be understood with the model, the reason why these interference patterns are blinking is still unclear.

2. Experiment

C_{21} (99%) was purchased from Aldrich (Milwaukee, USA) and used without any further purification. With the aid of a spreading solution, the fatty acid was spread onto a subphase of ultrapure water (Nanopure-UV) at pH = 2. The spreading solution was made with chloroform (HPLC; Aldrich, Milwaukee, USA). HCl (Merck, Mexico) was used to modify pH.

All monolayers were prepared on a computerized Nima LB trough (TKB 2410A, Nima Technology Ltd, UK) using a Wilhelmy plate to measure the Π. All experiments were carried out in a dust-free environment. Temperature in the trough was kept constant with the aid of a water circulator bath (Cole-Parmer 1268-24, USA).

BAM observations were performed using a BAM1 (Nanofilm Technologie GmbH, Germany) with a spatial resolution of about 4 μm. The interface where the monolayer is deposited is illuminated at the Brewster incidence ($\sim 53^\circ$) with a p-polarized beam from a He–Ne laser. A lens receives the reflected light. Afterwards, the reflected light is sent to a polarization analyser with the aid of a mirror that makes a specular inversion of the image. Finally, the polarization-analysed light is received by a CCD video camera to develop an image of the monolayer.

3. Interference patterns

LO can be observed in the images of figure 1, coming from the same area of observation in the monolayer. These images were obtained from our VCR tape observation records. Π relaxes as

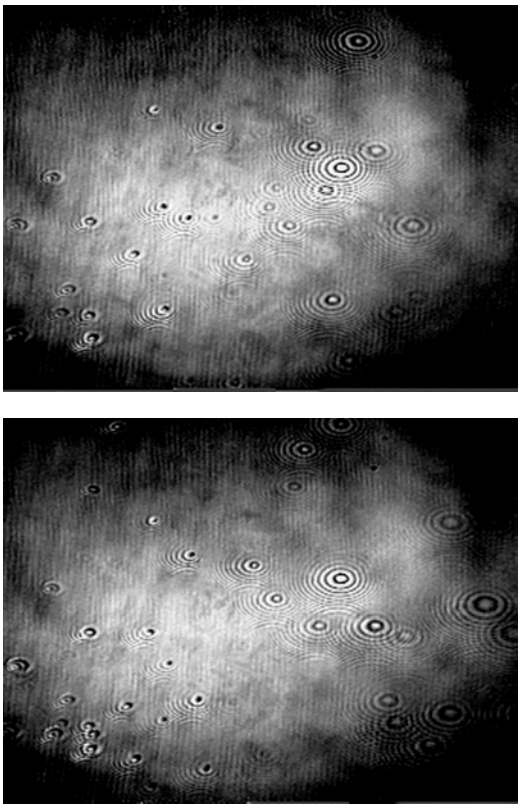

Figure 1. BAM images of a C_{21} monolayer at CS phase, showing interference rings that suddenly appear and disappear in the same place on the monolayer. The elapsed time from the first image (*a*) to the second one (*b*) is less than 1/6 of a second. In both figures, the horizontal breadth corresponds to about 850 μm.

a function of time when LOs are present. The larger the pressure drops the larger the number of LOs in the monolayer. BAM reveals the formation of typical multilayer structures, as pressure goes down after long periods of blinking. However, at the very beginning, when LOs are just starting, it is possible to see the formation of an irregular white domain at the place where the interference rings are blinking. The oscillations remain for a long time until pressure relaxes; in some cases Π relaxes continuously to values close to 0 mN m^{-1} after 24 h. We were unable to measure a characteristic time of oscillation for LOs, because the period can extend from less than 1/30 of a second to a few oscillations per second, depending on the chosen LO. LO can start at low temperatures ($\sim$2–6 °C) and at low pressures ($\sim$12 mN m^{-1}) compared with the collapse pressure. However, as the pressure is increased, the number of oscillation sites increases quite notoriously. Compressions at very slow rates present fewer LOs. If the crystalline phases are reached by decreasing temperature slowly, starting from a more fluid phase, LOs never show up. However, some static interference rings remain, i.e. fixed defects that are not blinking on the monolayer. Heat treatment also lowers the number of LOs, but many frozen defects can be observed; many of these are static interference rings. All these features led us to conclude that during a normal compression process, there is not enough time for a proper relaxation in these crystalline states. Thus, an adequate matching of the different order parameters at the grain boundaries of crystalline phases of the monolayer does not occur.

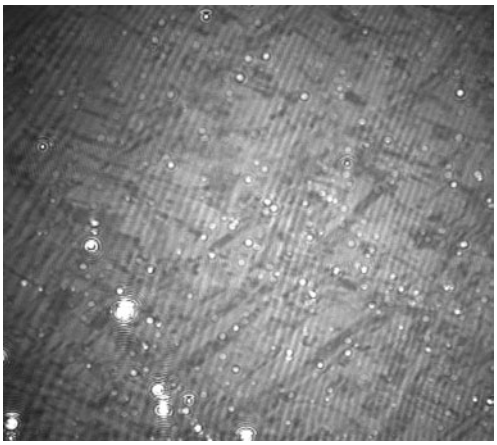

Figure 2. Multilayer defects mainly along the domain boundaries in an all-in-focus BAM image of a C_{21} monolayer at CS phase when LOs are present (obtained with an NFT I-Elli2000 imaging ellipsometer, Nanofilm Technologie GmbH, Germany).

Therefore, there are large areas with a high density of defects and, consequently, of stress. The monolayer apparently relaxes, expelling matter from the monolayer. Some evidence of this can be seen in figure 2, where most of the defects are found at the border of the domains. LO seems to be the mesoscopic evidence of the expulsion of matter.

Notwithstanding the picture given above, a question remains: what are these patterns that remind us of interference rings, which are blinking when observed with BAM? Are they consistent with the events related to the expulsion of matter out of the monolayer just described? Galvan-Miyoshi *et al* [22] found, with atomic force microscopy, a homogeneous surface covered with granules appearing like irregular discs in transferred monolayers on mica, when the monolayers presented a high population of LOs. The grains had a mean grain size in the order of 6 μm and with typical heights in the range of 0.015 μm. These results agree with the event of expulsion of matter out of the monolayer. However, why do we see something like interference rings as in the case of thick films? In that case, some portion of the light is refracted and another reflected, at the surface of the thick film. The refracted light is subsequently reflected in the next lower boundary (water subphase). An interference pattern is obtained when the two portions of light are mixed because of the difference in optical path. However, this could not be the case for the granules found by Galvan-Miyoshi *et al* [22]. Disc heights could not allow interference in the way just mentioned, because granules are illuminated with light of wavelength $\lambda = 632.8$ nm from the Brewster angle microscope. The granules are too short for the wavelength of the light! Therefore, we must look for an alternative explanation.

4. Model

Brewster angle microscopy [23,24] is a technique based on the study of the light reflected from an interface illuminated at the Brewster angle, by a p-polarized laser beam. When the angle of incidence of the laser beam is at the Brewster angle, there is no light reflected from a clean and perfect interface, i.e. one where the refractive index changes abruptly from one medium to another. At a real interface, which has a transition region where the refractive index changes smoothly from one value to another, the reflected intensity at the Brewster angle is a minimum,

but it does not vanish completely and also depends strongly on molecular anisotropy. Thus, a monolayer on an interface is able to produce a slight reflection of light. In tilted phases, the anisotropy is relatively strong to have enough light reflection to make quite visible the mosaic of textures because of tilted domains in different directions. In untilted phases with rectangular lattice symmetry, textures are also visible, but with much less contrast. On the other hand, multilayer structures reflect very large quantities of light as compared with a monolayer. This is very easily observed with a Brewster angle microscope.

Mesoscopic granules laying down on the monolayer are made of several layers of amphiphilic molecules, which will reflect relatively large quantities of light. In contrast, the monolayer will be working as an almost opaque screen, because of its relatively low reflectivity. It is evident that this situation is equivalent to that formed by a black screen with an aperture, where light is coming from below the black screen, at the Brewster angle, and observed in the far field. In this situation, Fraunhofer diffraction must be observed, because of the finite size of the light source (aperture or reflecting disc). The light intensity distribution for a circular diffracting aperture or for a disc, of radius s, reflecting light can be calculated with the formula for diffracted electric fields in the far-field approximation [25]. The light intensity distribution, on an observation plane perpendicular to the reflected Brewster angle beam, can be written as [22]

$$I_{relative}(x', y') = \left\langle \frac{I(x', y')}{I(\theta_B)} \right\rangle = \left[\frac{2J_1(ks\rho/R)}{ks\rho/R} \right]^2. \tag{1}$$

This distribution is known as the Airy pattern. J is a Bessel Function; θ_B is the Brewster angle. $\rho^2 = x'^2/\sec^2\theta_B + y'^2/\csc^2\theta_B$, where x' and y' are coordinates defined on a plane of observation perpendicular to the reflected Brewster angle beam. x' is along the incidence plane and y' is perpendicular to the incidence plane. $I(\theta_B)$ is the intensity in the direction of the reflected Brewster angle beam, where x' and y' vanish. $I_{relative}(x', y')$ starts at a maximum intensity equal to unity and decays as the Airy pattern. This approximation is not valid for $ks < 1$ [25].

$I_{relative}(x', y')$ must have constant values at the geometrical loci where x' and y' vary in such a way that $\rho^2 =$ constant, i.e. at ellipses. Therefore, the observed distribution is a deformed Airy pattern, since the rings where intensity is zero or a secondary maximum are elliptical in shape. The semimajor axis of the central disc, as well as of the different n black rings, can be obtained directly from (1). They can be written in the following form [22]:

$$a_n = \frac{J_1(\alpha_{1n})}{\pi \cos\theta_B} \frac{R\lambda}{2s}. \tag{2}$$

The secondary maxima, i.e. the semimajor axis of the n white rings, can be written with the equation [22]

$$a'_n = \frac{J_2(\alpha_{2n})}{\pi \cos\theta_B} \frac{R\lambda}{2s}. \tag{3}$$

In both equations, α_{mn} are the zeros for the Bessel function J_m and n is taken from inside outwards.

5. Results and discussion

Several measurements were made to show that the mesoscopic granules laying down on the monolayer are reflecting light following the intensity distribution given by equation (1). Below, we present our results and a discussion of them.

Table 1. Calculated and experimental average values for the semimajor axis ratios for white and black rings, and percentage deviation from the experimental values.

	White rings (a'_n/a'_1)			Black rings (a_n/a'_1)		
n	Theory	Experiment	%	Theory	Experiment	%
1	1	1	0	0.74	0.53	38.0
2	1.64	1.75	6.5	1.36	1.42	4.3
3	2.26	2.40	5.5	1.98	2.10	5.9
4	2.88	2.94	2.1	2.59	2.67	3.1
5	3.5	3.44	1.6	3.21	3.21	0.1
6	4.11	3.98	3.2	3.82	3.74	2.1
7	4.73	4.46	6.0	4.43	4.24	4.6

(1) A very precise test can be given *measuring the semimajor axes* of the observed rings in single patterns. The elliptical rings in an Airy pattern originated by light reflection from a disc of a specific size must have fixed values. They are given by expressions (2) and (3). This test could be very precise, if some internal distance in the pattern were taken as a reference distance, because of BAM introduces magnification factors. One of them depends directly on the distance from the pattern to the focal plane, and the other originates from the instrumentation. In the latter case, images at an observational plane are larger in the plane of incidence than in the direction perpendicular to the plane of incidence. However, the instrumental amplification factors must be the same for each ring in a given pattern. Therefore, if semimajor axis ratios in a pattern are measured, taking one specified semimajor axis as a reference, then the amplification factors would cancel and there is no need to calculate them explicitly. Here, we used ratios of the semimajor axis for each ring (black or white) to the semimajor axis of the first white ring a'_1. The semimajor axis ratios for n black or n white rings can be calculated using equations (2) and (3):

$$\frac{a_n}{a'_1} = \frac{J_1(\alpha_{1n})}{J_2(\alpha_{21})}, \qquad \frac{a'_n}{a'_1} = \frac{J_1(\alpha_{1n})}{J_2(\alpha_{21})}. \tag{4}$$

Table 1 presents the calculated values for the semimajor axis ratios of the first seven white and black rings in a pattern, as well as the average measurements for the same semimajor axis ratios made on electronically amplified BAM images. We used a set of 33 randomly chosen patterns from different monolayer preparations to obtain averages. The agreement is quite good, since deviations from the calculated values are in the range of a few per cent, except for the first black ring. For the seventh ring, the statistics is not so good because in some of the patterns it was not possible to measure this ring. The first black ring is the ring that limits the central white disc in an Airy pattern. In our case, when the pattern images are amplified, we observed that the perimeter of several central white discs is not perfectly circular. Shades of grey suggest polygonal shapes circumscribing the discs. We believe that this effect is because the actual granules are not circular. Thus, these noncircular perimeters made difficult the determination of where to take the end of the central disc and consequently the central part of the first black ring. This explains the observed mismatch. Another important outcome (not shown) is that the blinking patterns give the same semimajor axis ratio results as the fixed patterns. This suggests that around a fixed pattern the expulsion of matter has ended, probably because the monolayer has locally relaxed.

(2) *Bright intensity measurement in the patterns*. In this test, we measured the brightness intensity for many blinking patterns on electronically amplified BAM images. The levels of intensity to be analysed are quite different in magnitude. For instance, the central white disc in an Airy pattern is two orders of magnitude larger than the first white ring. Therefore,

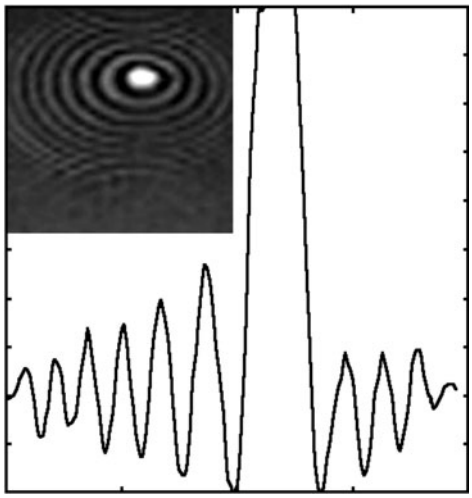

Figure 3. The brightness intensity distribution in arbitrary units along a line crossing a pattern horizontally in the middle.

this is a semiquantitative test because the capability of a BAM for this kind of light intensity measurement is limited. An example of the brightness intensity measurements is presented in figure 3. Here, an electronically amplified BAM image of a pattern (inset in figure 3) was digitized to obtain a bitmap image. The brightness was obtained as a normalized grey scale for each pixel (0 for black and 1 for white), using Matlab software. In this figure, we present the intensity along a line crossing the pattern horizontally in the middle. The central disc is quite intense until it reaches the white level saturation. In the next rings the base line is not horizontal; however, the brightness intensity of the peaks decreases as the ring number increases, and the intensity of the secondary maxima has the same order of magnitude, in agreement with the model. Notwithstanding the precision of this test, we think that the agreement is quite good.

(3) *Direct comparison between actual and calculated patterns*. An algorithm for calculating the light intensity distribution without approximations was implemented. Figure 4(*a*) presents a calculated light intensity distribution pattern for a disc of radius $s = 20\ \mu$m, just as would be observed in the monitor of our BAM, i.e. including the amplification factors. We are using a grey scale where the brighter the area the greater the value of the intensity distribution. In figure 4(*b*), we present the superposition of the calculated pattern and an actual pattern taken from our video recordings. The fitting is quite remarkable. This calculation seems to indicate that our model is able to reproduce the observed patterns.

(4) *Fraunhofer and Fresnel patterns*. The patterns are modified when they cross the screen of the monitor from one side to the other during the observations. First, on the right-hand side the patterns are large, very well defined. As far as we move the microscope, to leave the patterns at the centre of the screen, the patterns are smaller. When we are close to the area on the monolayer where the BAM is in focus, the white centre of the pattern changes to a black centre. Finally, when we move along the monolayer in such a way that the patterns are to the left of the area that is in focus, the definition of the patterns is lost. These events can be easily explained with our diffraction model. In our BAM, the images are mirror inverted. Therefore, those areas on the screen that are seen on the right-hand side of the focused area are actually on the left of the focal plane and vice versa. Thus, patterns that are not in focus correspond to patterns that are on the right of the focal plane and cannot be seen in focus. In contrast, the well defined patterns are on the left of the area that is in focus and, in addition, far from

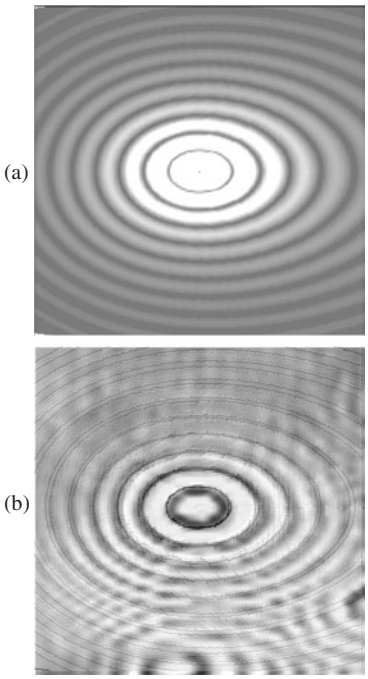

Figure 4. (*a*) Calculated light intensity distribution pattern for a disc of radius $s = 20$ μm, as would be observed in the monitor of our BAM. (*b*) Superposition of the calculated and an actual pattern taken from our video recordings.

the focal plane. From this plane, the Fraunhofer diffraction patterns are taken by the lens to be focused in the CCD camera. As we move the BAM to leave the patterns in the area that is in focus, i.e. at the focal plane, the diffraction patterns are taken very close to or at the finite source of light. Therefore, the observed patterns must be Fresnel diffraction patterns [26]. One important characteristic of a Fresnel pattern is to have a black centre.

Notwithstanding the success of our model for explaining the optical nature of the patterns, it does not help us to understand the origin of the blinking. As mentioned above, crystalline phases of monolayers apparently relax, expelling matter, and LO seem to be the mesoscopic evidence of these events. However, the mechanism of how the expulsion of matter and the blinking are related is not clear. Understanding this relationship could be of interest, because it could give a procedure for observing stress relaxation in crystalline phases, through the measurement of distribution and frequency of blinking patterns, as well as the way they become fixed along the monolayer. We are considering several possibilities; however, more work has to be performed.

(i) *Discontinuous process of expulsion of matter from the monolayer*. Here, LO could be the optical evidence of a process of successive steps of expulsion of matter and discontinuous granule growth using the expelled material. In this case, the diameter of the granules must be changing discontinuously after each successive expulsion. The granules being formed and reformed could cause the blinking through reflecting light discontinuously due to the abrupt changes during the reformation of the granules. However, it is difficult to explain why this process has to be mesoscopically discontinuous in order to see patterns appearing and disappearing, in particular when the period of oscillation is very short.

(ii) *Fluctuation of granule dielectric constant*. In this case, when the granules are formed,

their lattice organization is fluctuating, trying to reach the most stable configuration. As a consequence, the dielectric constant and the index of refraction of the granules should be fluctuating too. This would give rise to reflectivity fluctuations, which could be responsible for the blinking. However, we do not understand why this reflectivity fluctuation seems to be periodic for relatively long periods of time.

(iii) *Grain wobbling*. In some cases, the reflected light coming from the patterns blinks, but without disappearing completely, in such a way that they seem to be swinging or wobbling. One explanation could be that in areas with a high density of defects and, consequently, stress and energy, the matter which is sent out from the monolayer produces large perturbations, in such a way that the granules that are on the monolayer are wobbling. In some cases this swinging is not so large, but in others this wobbling could make the reflected light miss the CCD camera entrance, giving the impression that they are blinking. The drawback here is that the estimated movements of the discs in order that the CCD camera misses the reflected light must be too large.

The blinking of interference patterns seems to be related to abrupt expulsion of material from the monolayer, although the actual mechanism is not known; it is a new mechanism of evolving from two to three dimensions.

Acknowledgments

We acknowledge the partial support of DGAPAUNAM IN103598 and CONACYT 27513-E grants.

References

[1] Kaganer V M, Möhwald H and Dutta P 1999 *Rev. Mod. Phys.* **71** 779
[2] Rasing Th *et al* 1985 *Phys. Rev. Lett.* **55** 2903
[3] Lin B *et al* 1990 *Phys. Rev. Lett.* **65** 191
[4] Durbin M K *et al* 1994 *J. Phys. Chem.* **98** 1753
[5] Kenn R M *et al* 1991 *J. Phys. Chem.* **95** 2092
[6] Tippmann-Krayer P and Möhwald H 1991 *Langmuir* **7** 2303
[7] Schwartz D K, Schlossman M L and Pershan P S 1992 *J. Chem. Phys.* **96** 2356
[8] Schlossman M L *et al* 1991 *Phys. Rev. Lett.* **66** 1599
[9] Kaganer V M *et al* 1995 *J. Chem. Phys.* **102** 9412
[10] Shih M C *et al* 1992 *Phys. Rev.* A **45** 5734
[11] Kjaer K *et al* 1989 *J. Phys. Chem.* **93** 3200
[12] Bohanon T M *et al* 1990 *Phys. Rev.* B **41** 4846
[13] Schwartz D K and Knobler C M 1993 *J. Phys. Chem.* **97** 8849
[14] Rivière-Cantin S, Hénon S and Meunier J 1996 *Phys. Rev.* E **54** 1683
[15] Rivière S *et al* 1994 *J. Chem. Phys.* **101** 1045
[16] Ramos S and Castillo R 1999 *J. Chem. Phys.* **110** 7021
[17] Lipp M M *et al* 1998 *Phys. Rev. Lett.* **81** 1650
[18] Ries H E 1979 *Nature* **281** 287
[19] Schief W R, Hall S B and Vogel V 2000 *Phys. Rev.* E **62** 6831
[20] Kampf J P *et al* 1999 *Science* **283** 1730
[21] Vollhardt D 1993 *Adv. Colloid Interface Sci.* **47** 1
[22] Galvan-Miyoshi J, Ramos S, Ruiz-García J and Castillo R 2001 *J. Chem. Phys.* **115** 8178
[23] Höning D and Möbius D 1991 *J. Phys. Chem.* **95** 4590
[24] Henon S and Meunier J 1991 *Rev. Sci. Instrum.* **62** 936
[25] Jackson J D 1975 *Classical Electrodynamics* 2nd edn (New York: Wiley) ch 9
[26] Saleh B E A and Teich M C 1991 *Fundamentals of Photonics* (New York: Wiley) p 966